AR-010-327

DSTO

Assessment of Underwater Blast Effects on Scaled, Submerged Cylindrical Objects

Michael Chung and John Brett

DSTO-TR-0575

APPROVED FOR PUBLIC RELEASE

DEPARTMENT OF DEFENCE

DEFENCE SCIENCE AND TECHNOLOGY ORGANISATION

Assessment of Underwater Blast Effects on Scaled, Submerged Cylindrical Objects

Michael Chung and John Brett

Maritime Platforms Division
Aeronautical and Maritime Research Laboratory

DSTO-TR-0575

ABSTRACT

The underwater detonation of large explosive charges close by a target, produce effects that are devastating to vessels such as ships and submarines and in addition, provide a means to neutralise threat sea-mines. The roles of the underwater shock wave, flow and bubble in the damage process are not as yet, clear. We present results of an experimental study visualising the effects of underwater explosions on scaled, submerged cylindrical objects that represent submarines and sea-mines. Significant structural damage to the cylinder occurred with the passage of the shock wave. During this period, the bubble of detonation products failed to expand sufficiently to contact the cylinder. Some evidence is available to suggest that the principal damage mechanism can be attributed to shock wave interaction and not water flow effects. Cavitation was created by the response of the cylinder to the shock wave and by the reflection of the shock wave from the bubble. Estimation of the effective loading period of the shock wave was made from these effects.

DEPARTMENT OF DEFENCE

DEFENCE SCIENCE AND TECHNOLOGY ORGANISATION

Published by

DSTO Aeronautical and Maritime Research Laboratory
PO Box 4331
Melbourne Victoria 3001 Australia

Telephone: (03) 9626 7000
Fax: (03) 9626 7999

AR-010-327
September 1997

APPROVED FOR PUBLIC RELEASE

Assessment of Underwater Blast Effects on Scaled, Submerged Cylindrical Objects

Executive Summary

MHCPD requires advice on the suitability and performance of mine disposal charges carried by the Mine Hunter Coastal, Mine Disposal Vehicle. In addition, SPD requires a computer based submarine vulnerability assessment capability based on regional ASW threats with HMAS Collins as the primary target.

As a consequence of these requirements, AMRL needs to 1) evaluate factors of an underwater explosion that will contribute to the sympathetic detonation of mine like charges and 2), further develop its submarine vulnerability/survivability assessment capability to provide Navy with the capability to determine submarine survivability under a range of senarios and threat environments.

These assessment capabilities will improve as our understanding of the physical processes involved with the interaction of an underwater explosion with a nearby target improves. To achieve these ends, an experimental program to determine the parameters, critical in the damage mechanism to targets such as submarines and sea-mines were devised.

Presently, it is not clear whether the major damage sustained by the target can be attributed to the underwater shock wave or the expansion and subsequent collapse of the bubble. To visualise these effects, experiments were conducted in a small scale experimental facility using a water filled transparent aquarium and a Cordin rotating mirror camera. Small explosive charges were detonated in the aquarium, in close proximity to scaled cylinders representing sea-mines and submarine's hulls. The expansion of the shock wave and bubble were recorded by a Cordin camera over a period of approximately 100 μs.

The results show the shock wave rapidly separating from the expanding bubble before interacting with the target. Damage sustained by the target was attributed to the passage of the shock wave and not to the expansion of the bubble. Cavitation was observed close to the surface of the cylinders and was caused by the rapid reaction of the surface of the cylinder to the passing shock wave. The measurement of the expansion of the shock wave has allowed the shock wave's velocity incident onto the target and the subsequent reaction velocity of the surface of the target to be calculated. These results will allow near field and far field effectiveness of underwater explosions against Collins, other regional submarines and sea-mines to be evaluated.

Authors

Michael Chung
Maritime Platforms Division

Michael Chung joined DSTO in 1969 and has worked widely in the fields of Applied Physics at AMRL. Recent work has investigated the effects produced by the interaction of underwater shock waves with explosive materials and simple structures. He is an Associate of the School of Mines Ballarat and graduated from the Royal Melbourne Institute of Technology in Applied Physics.

John Brett
Maritime Platforms Division

John Brett was awarded a Ph D in Astrophysics from the Australian National University in 1988 following which he spent five years engaged in pastoral research at universities in England, Sweden and Australia. He joined the Maritime Platforms Division (then SSMD) of AMRL in 1993. Since then he has been researching underwater explosive damage effects and associated aspects of submarine vulnerability.

Contents

1. Introduction

The underwater detonation of a large explosive charge produces a spherical shock wave and a bubble of gaseous products at high temperature and pressure. In the near-field, close to the point of detonation, the initial velocity of the shock wave is typically 3000 ms^{-1} [1] with a corresponding pressure level of the order of 23000 atmospheres. Both the velocity and the pressure level of the shock wave rapidly decrease with distance until in the far-field (> 5 charge radii) [1], they approach acoustic values and the principle of similarity can then be used to predict the shock wave's characteristics. Simple analysis of the propagation of such a wave shows that the water is left with an outward velocity, following the passage of the shock wave [2].

The bubble of gaseous products expands until the pressure within the bubble falls below a value determined by the sum of atmospheric and hydrostatic pressure. The expansion causes an outward flow of water; the velocity of which is determined by the pressure within the bubble plus the afterflow characteristics of the water caused by the passage of the shock wave. Eventually, the pressure difference described above reverses the motion of the boundary of the bubble, causing it to collapse. The expanding shock wave and bubble quickly become separated because of the shock wave's greater velocity [1] and as a result, a target close-by will be subjected in turn, to each effect.

The subsequent shock loading experienced by a vessel may be sufficient to buckle or rupture its hull, and can produce extensive damage to internal equipment or, at close range, initiate sympathetic detonation in the explosive filling of a sea-mine.

The effects produced by bubbles on vessels are devastating. Evidence obtained from full scale ship trials [3] and the incident with USS Roberts [4] have indicated that the bubble produced beneath the keel of a ship will induce whipping motion in the ship's structure, leading to the breaking of its hull grider. Scaled testing of small underwater explosives near a rigid submerged cylinder indicates that under suitable conditions the bubble will collapse forming a jet of water that completely penetrates the bubble and impacts on the structure [5]. This collapse has been successfully modelled by assuming the bubble evolves into a toroid form; the flow domain being doubly connected [6]. However, additional work is required to experimentally determine the velocity of water jets that will successfully penetrate the hull of a vessel.

Of particular interest are the effects on a submerged vessel of processes that are predominate in the early stages of an underwater explosion. It is not clear if the principal cause of damage may be attributed to the shock wave, the after flow caused by the passage of the shock wave or the flow caused by the expansion of the bubble. A better understanding of the interaction of these physical processes with a nearby target will assist in the development of computer models vital to vulnerability studies of submarines and surface ships.

Similarly, the identification of the major damage process to sea-mine like structures will allow the critical parameters of that particular process to be investigated, eliminating further speculation on the roles that the other processes play in the neutralisation of sea-mines.

Consequently, an investigation was undertaken to visualise the effects of underwater explosions on scaled, submerged objects. This paper discusses the interaction of underwater blast effects with cylindrical structures and presents results from the scaled testing of cylinders representing submarines and sea-mines.

2. Shock Wave Interaction with a Boundary and the Production of Cavitation

For normal incidence of a shock wave onto an arbitrary boundary between two media, one shock wave is transmitted across and another is reflected from the boundary. The type of boundary is determined by the acoustic impedance of the media and the effects at the boundary are determined by the principles of conservation of mass and momentum across the boundary.

For a rigid boundary where the shock wave is incident onto a medium whose acoustic impedance is very much greater than that through which it passes, no transmitted wave will occur across the boundary. The resistance of the boundary annuls the normal flow set up by the incident wave. This effect will result in no movement of the boundary and a reflected wave that increases the compression along the boundary.

At a boundary free to move, the shock wave is incident onto a medium whose acoustic impedance is less than that through which it passes. A transmitted and reflected wave can occur and no resistance to compression can exist along the boundary. The reflected wave must leave the fluid in its original state of compression. This results in a rarefaction wave whose magnitude reduces the pressure in the medium to its original value and produces flow normal to the boundary, producing a movement of the boundary. The nett pressure behind the incident wave will become negative due to the rarefaction and a region of cavitation will form. The time taken for a negative nett pressure to be achieved by the rarefaction moving through the incident wave is the effective loading time of the incident shock wave. When cavitation forms, the pressure on the boundary is released and the motion of the boundary will be modified.

The magnitude of shock waves reflected and transmitted at an arbitrary boundary between two media of similar acoustic impedance may be determined from material Hugoniots as follows.

The pressure P of a shock wave of velocity U, travelling in a medium of density ρ_0, is given by [7];

$$P - P_0 = \rho_0 U u \quad (1),$$

where u is the particle velocity of the shock wave, and P_0 is the ambient pressure in the medium. The relationship between U and u in a medium is determined experimentally and in most cases is linear [8, 9]. The Hugoniot for water is given by [10];

$$U = 1.483 + 25.306 \log_{10}(1 + u/5.190) \quad (2)$$

and a Hugoniot for steel is given by [9];

$$U = 4.58 + 1.49u \quad (3),$$

where U and u are measured in *km/s*.

When such a shock wave interacts with a boundary between two media, a reflected shock is produced in one medium and a transmitted shock is produced in the other. If the pressure and particle velocity of the incident shock wave prior to the interaction are P_1 and u_1 respectively, then the characteristic of the reflected wave must also pass through this initial state. The $P-u$ characteristics (Hugoniots) of the incident and reflected waves are illustrated in Figure 1.

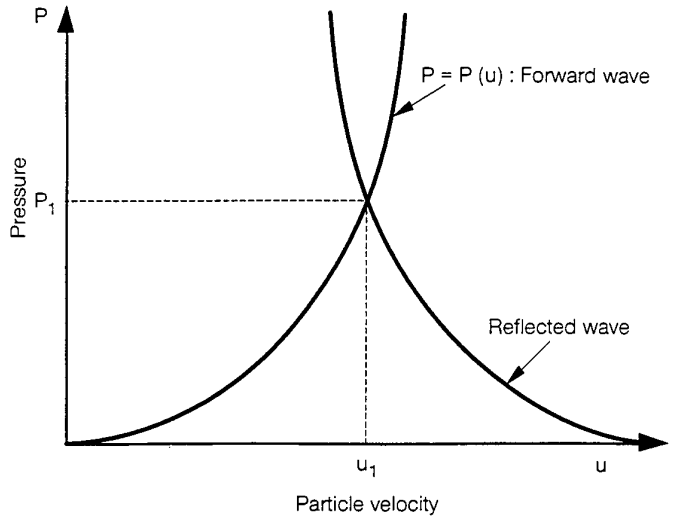

Figure 1. Forward and Reflected P-u characteristic curves for a typical medium

Because the pressure and particle velocity across the boundary between two media are continuous, the pressures and particle velocities behind the reflected and transmitted waves will be equal. This condition only occurs at the intersection of the characteristics of the reflected (in medium 1) and transmitted (in medium 2) waves. This condition is illustrated in Figure 2.

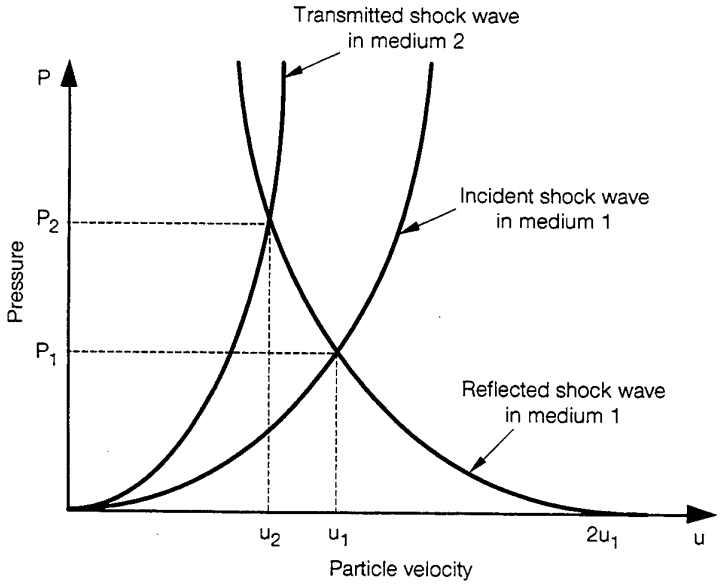

Figure 2. Impedance matching method of determining pressure and particle velocity behind waves reflected at a boundary.

The slopes of the P-u characteristics determine the relative magnitude of the reflected and transmitted waves and if the boundary is free to move, a rarefaction rather than a shock is produced in medium 1. The rarefaction effect produces tension within medium 1 and for the case of water, which cannot withstand this tension, a region of cavitation is formed [2]. For the condition shown in Figure 2, the pressure and particle velocity behind the two waves are P_2 and u_2 respectively.

The interaction of an incident shock wave with a free stationary, simple structure suspended in water may be described in terms similar to those of Figure 2. Here, the incident shock wave will produce either bodily movement of the structure or movement of the surface of the structure as it deforms. Either way, a reflected wave of magnitude P_2 will be transmitted back into the water from the accelerated surface of the structure and the particle velocity u_2 of the water in contact with the structure is equal to the velocity of the structure. The onset of cavitation indicates that the pressure in the incident shock wave is zero and the shock wave will no longer affect the motion of the structure.

These conditions are illustrated in Figure 3 and only apply to the bodily movement of the structure; the reflection/transmission P-u characteristic used for the structure is a material Hugoniot, which does not account for deformation effects.

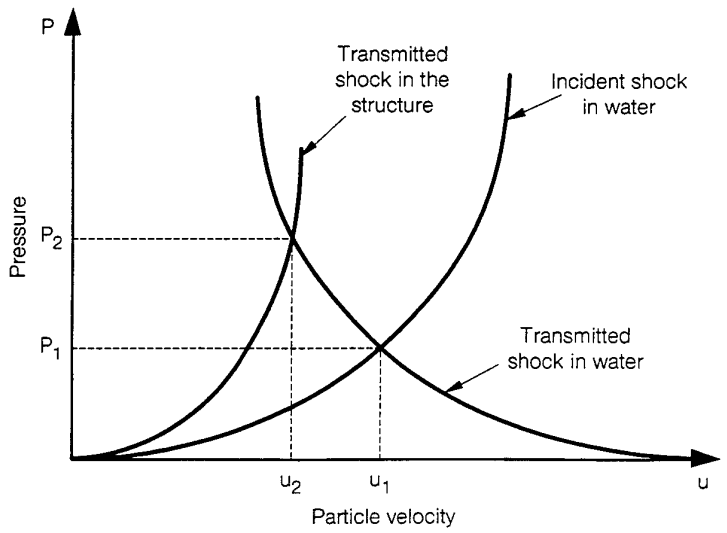

Figure 3. Impedance matching method of determining effects due to motion of a structure, freely suspended in a medium.

3. Test Description

The experiments were conducted in a small scale explosive test facility [11] shown schematically in Figure 4. This facility utilises a firing chamber designed for a maximum 2.25 kg charge mass, a Cordin model 330 rotating mirror camera and a transparent aquarium, illuminated by an Argon light box. The chamber has 7 horizontal viewing ports that allow flexibility in the geometrical arrangement of the aquarium and the optimisation of the light path through the chamber. The explosive charge and target were positioned in the aquarium and rigidly supported in the Cordin camera's field of view. The camera was arranged to view the subject via an image rotator and two mirrors. The first of these mirrors was surface coated to provide the best available image quality and was mounted on a stand outside the firing cell. The second mirror was placed inside the firing cell, and hence was expected to be destroyed with every shot. The firing cell window was a sheet of 25 mm thick PMMA, faced on the inside with a 3 mm thick sheet of PMMA.

The subject was back illuminated by an explosive/Argon flash bomb. Exploding Bridge Wire detonators (EBW) RISI 501 were used in both the flash bomb and pentolite donor; these detonators were selected for performance, safety and reliability of functioning. The EBW in the flash bomb was triggered by a signal from the Cordin camera. A delay of 25-30μs was introduced between firing the flash bomb and pentolite charge to allow the light to build in intensity.

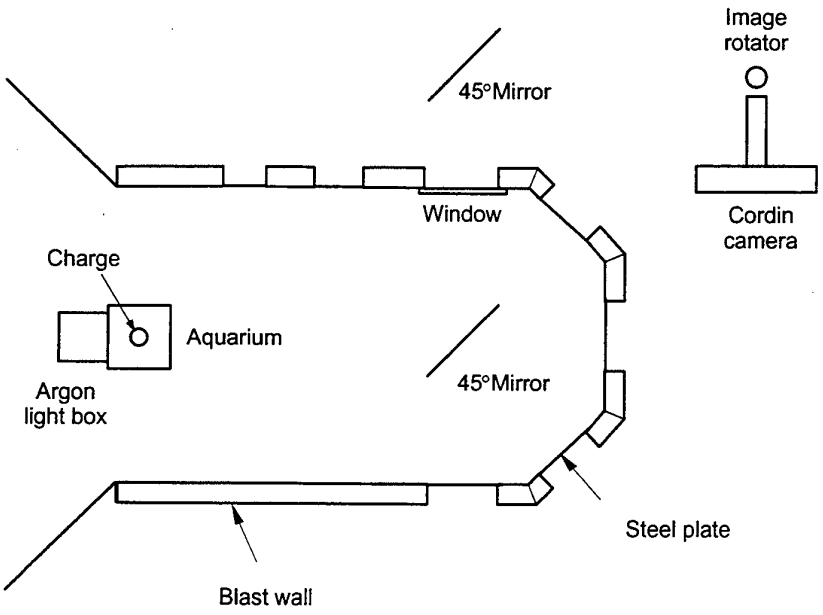

Figure 4. Plan view of the small scale explosive test facility showing the positions of the aquarium, light box and Cordin camera.

Steel cylinders represented sea-mines and spherical pentolite charges represented clearing charges. The cylinders were 160 mm long and 89 mm in diameter with wall thickness 6 mm. One cylinder was sealed at the ends and made water tight with perspex windows, the other sealed and made water tight with a disk welded to one end of the cylinder and a perspex window at the other end. The pentolite charges were of mass 0.5 kg and radius 42 mm. The stand-off distance of the cylinder from the charge was scaled so that the separation was 2.25 charge radii, a distance typical of mine clearing operations. The effect of shock waves on cylinders, one whose longitudinal axis was parallel, and the other whose axis was at right angles, to the radial direction of the shock wave was recorded by the Cordin camera. The framing records were used to visualise the interaction of the shock wave with the cylinders whilst the streak records were used to determine positional and velocity data of the shock wave and bubble surface.

A further series of experiments were directed towards a study of the damage mechanisms affecting submarine hulls. For this study we have attempted to roughly scale a typical torpedo warhead - submarine hull interaction by applying Hopkinson's scaling rules to both the diameter and wall thickness of the cylinder and the mass of the explosive. While this approach scales important factors such as the impulse and energy of the interaction we appreciate that not all attributes of the full scale interaction can or have been scaled. In particular the bubble diameter versus hull diameter is not correctly scaled, although this could be achieved by adjusting the air pressure on the surface of the aquarium. Furthermore it is acknowledged that the

details of the target cylinder are not a true representation of a submarine hull; in particular a real hull includes stiffener ribs and is constructed from higher yield stress steel. Both of these differences will make a real submarine hull considerably less responsive to shock loading than our experimental target cylinder. However, the primary purpose of this experiment was to generate real, experimental data for application to the development of a computational damage prediction capability via FEA techniques. For the initial development of this capability a simple responsive structure was desirable.

In the small scale experiment described here we detonated a 10 gm charge midway between the ends of the cylindrical target and at a distance of 75 mm from its surface. The centre of both target and charge were submerged at a depth of 300 mm. The simple cylindrical target was a 500 mm long cylinder of 300 mm diameter constructed by rolling 2 mm mild steel sheet and joining it along its length with a continuous weld. The open ends were sealed and made watertight with perspex windows which permitted observation of the internal deformation. The cylinder was orientated with this weld away from the charge. The experiment was filmed along the cylinder axis with the field of view centred on the cylinder wall closest to the charge. The orientation of the charge and cylinder is shown schematically in Figure 5.

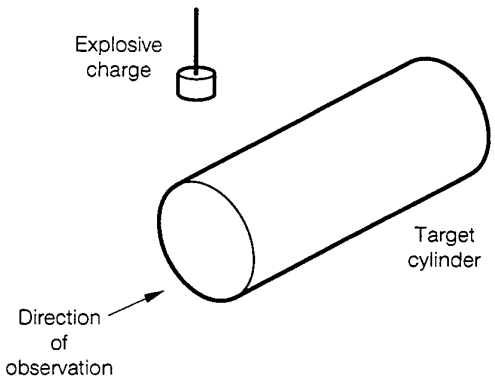

Figure 5. Experimental arrangement for 'submarine' hull experiment.

A spherical explosive charge of 10 gms of PE4 has a diameter of approximately 20mm. Achieving the central detonation of such a small charge would be very difficult and accordingly, the PE4 charges were fabricated as right cylinders encased in a perspex charge and detonator holder. This charge was end initiated with an EBW whose physical size is comparable to that of the cylinder. This arrangement is shown schematically in Figure 6. The effect of the geometry of such a small charge on the underwater shock wave produced by its detonation is not clear. To investigate the geometric effects of small charges, a separate experiment was conducted to observe the development of the shock wave and expansion of the bubble from the detonation of an isolated charge.

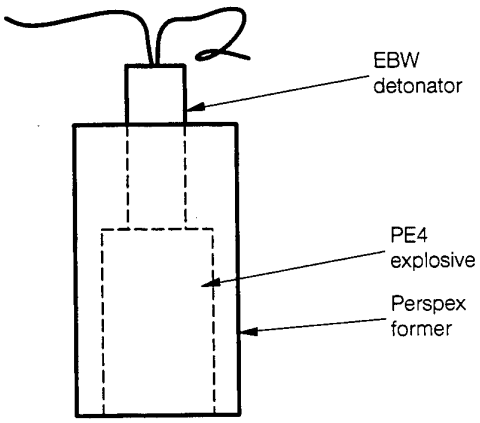

Figure 6. Schematic of the right cylindrical PE4 charge.

4. Results and Discussion

4.1 Cylinders representing sea-mines

The interaction of a spherical shock wave with an air-filled steel cylinder whose longitudinal axis is parallel to the radial direction of the shock wave was recorded by the Cordin camera. This event is illustrated by selected framing records shown in Figure 7. The incident shock wave can be seen propagating through the water, interacting with the flat steel plate at the end of the cylinder and propagating along the length of the cylinder. There is no clear evidence in the framing records of either vortices produced by the incident wave as it diffracts around the cylinder or of the production of Mach reflection as the shock wave moves along the length of the cylinder. On contact with the cylinder, a reflected wave is produced behind the incident wave. This wave propagates into the expanding bubble of gaseous products and cavitation effects are seen to occur both at the end of the cylinder and near the surface of the bubble. From the framing records, cavitation is seen to be formed at the end of the cylinder, 18 microseconds after the incident shock wave contacts the cylinder.

The formation of cavitation in front of the bubble is detailed by the streak record shown in Figure 8. Cavitation is formed 13 mm from the surface of the bubble and 5.5 microseconds after the incident shock wave first interacts with the bubble. The early development of the shock wave and bubble are also illustrated by the streak record shown in Figure 8. The expansion of both the shock wave and the bubble's surface was digitised from this record and their paths in the distance-time plane are shown in Figure 9. Distance s is measured from the initial surface of the donor charge and time t is measured from the commencement of expansion of the donor charge. The continuity of the incident and reflected shock wave is disrupted because of the lack in clarity of the streak record. However, a general picture of the path of the shock wave incident onto the cylinder and bubble is clear. Figure 9 also indicates a period during which the

expansion of the bubble is retarded by the shock wave reflected from the steel cylinder. After approximately 40 microseconds, the expanding bubble merges with the cavitation effects and the paths of the shock wave and the surface of the bubble become indistinct.

The formation of cavitation on the steel plate at the end of the cylinder indicates that the reflected wave is one of compression rather than rarefaction. If the reflected wave was a rarefaction, it would produce a net negative pressure in the fluid in front of the cylinder as it moved through the incident wave and it would be here that cavitation would form. Instead, cavitation formed on the surface of the cylinder, indicating that tension in the fluid was produced by the rapid motion of the surface caused by the transfer of energy from the shock wave. From Figure 9, the gradient of the distance-time curve indicates that the velocity of the shock wave incident onto the cylinder is 2850 ms^{-1}. The particle velocity (flow) of this shock wave may be calculated from equation (2) as 687 ms^{-1}. Assuming that the density of water is 1000 kg/m^3 then the pressure in the water in front of the cylinder may be calculated from equation (1) as 2.0 GPa. On impact with the cylinder, the pressure and particle velocity are continuous across the boundary and impedance matching techniques will allow the characteristics of the reflected and transmitted shock waves to be calculated. Assuming the cylinder is constructed from steel 304, the magnitude of the transmitted and reflected shock waves at the cylinder's boundary is 4.8 GPa and the particle velocity across the surface of the cylinder is approximately 130 ms^{-1}. Thus, the surface of the cylinder will move backwards with an initial velocity of 130 ms^{-1}.

The formation of cavitation in front of the bubble can be explained in terms of the Hugoniots shown in Figure 3. The shock wave incident onto the surface of the bubble interacts with a boundary between a compressible (gas) and incompressible (water) fluid. The boundary acts as a free surface and a rarefaction wave pressure P_3, is produced on reflection that reduces the net pressure along the boundary to zero and a flow u_3, normal to the boundary. The normal flow produces movement of the boundary that is evident in Figure 9 as the retardation in the expansion of the bubble. The time taken for the formation of cavitation (5.5 microseconds) is a measure of the effective loading period of the incident wave and indicates that magnitude of the rarefaction is less than that of the incident wave. The Hugoniot of the bubble of gaseous products is unknown and similar calculations to those described above at the cylinder's surface cannot be carried out for the bubble's surface.

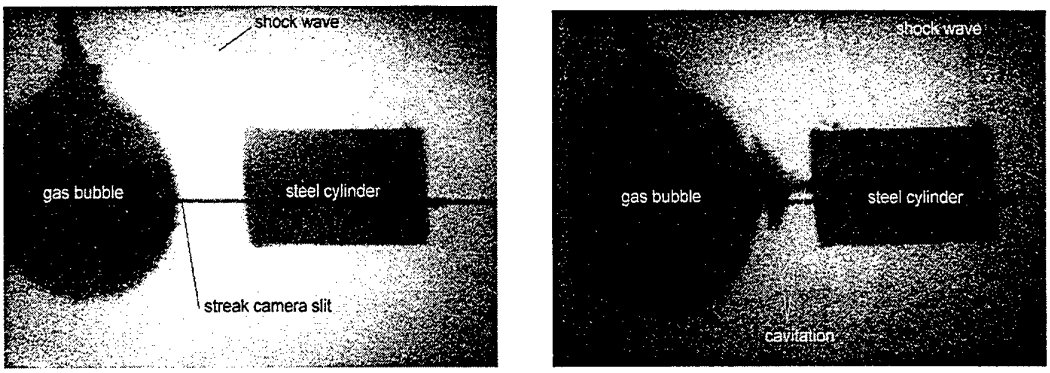

Figure 7. Frames showing the interaction of a shock wave with a cylinder after (a) 32, and (b) 47 *microseconds from detonation of the donor. The mirror period of the Cordin camera was 449.4 μs.*

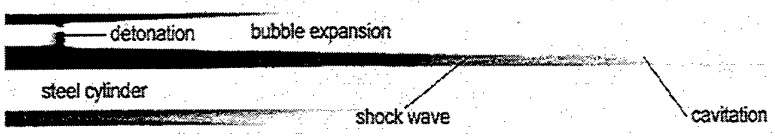

Figure 8. Streak record showing the formation of cavitation, the passage of shock waves between the donor charge and cylinder and the motion of the bubble's surface.

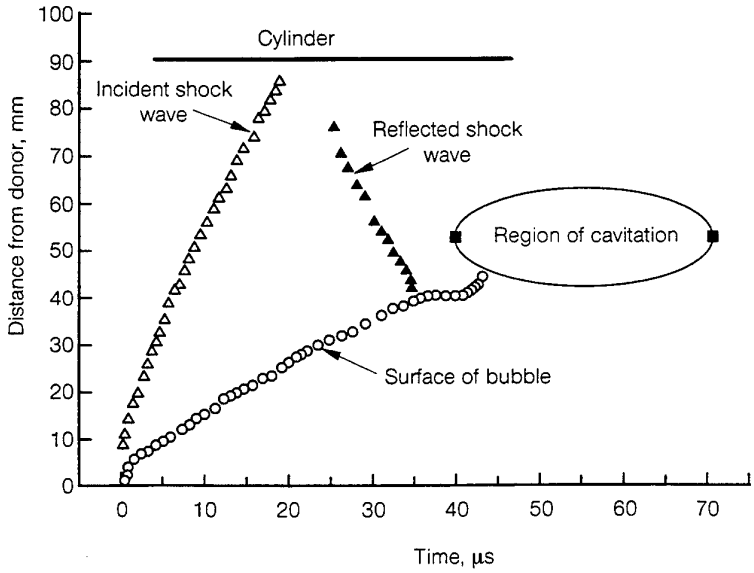

Figure 9. Paths of the shock wave and surface of the bubble in the s-t plane-Longitudinal interaction.

The complete set of framing records show that the cylinder begins to be crushed as the shock wave passes along its length with further damage occurring after the passage of the shock wave. The damage to the cylinder is complete, long before the bubble reaches the cylinder. These records also show that the relative position of the cylinder appears to remain constant during the life time of the experiment. On recovery of the cylinder after completion of the experiment, the steel plate at the end of the cylinder was found to be ruptured and the diameter of the cylinder varied along the length of the cylinder, the diameter being smaller at the end closer to the charge. The damaged cylinder is shown in Figure 10.

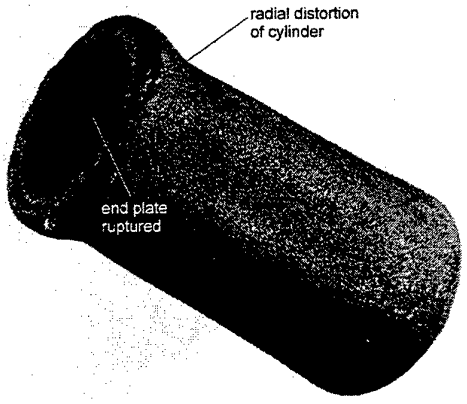

Figure 10. Damage resulting from the passage of the shock wave. The axis of the cylinder is parallel to the radial direction of the shock wave.

The deformation of the cylinder produced after the passage of the shock wave is thought to be due to the slow response time of the steel cylinder to events initiated by the shock wave. The lack of movement suggests that there is little or no effect on the cylinder due to water flow caused by the passage of the shock wave or the expected flow due to the expansion of the bubble. Because of this and the severity of the damage to the cylinder, we believe that the damage sustained is due to the shock wave alone and not due to flow effects.

Selected frames of the interaction of the shock wave with the air-filled steel cylinder at right angles to the radial direction of the shock wave was recorded by the Cordin camera and the event is shown in Figure 11. The ends of the cylinder were perspex disks, sealed to prevent the ingress of water and the orientation of the cylinder relative to the optical path of the Cordin camera allowed the passage of the shock wave through the cylinder to be observed.

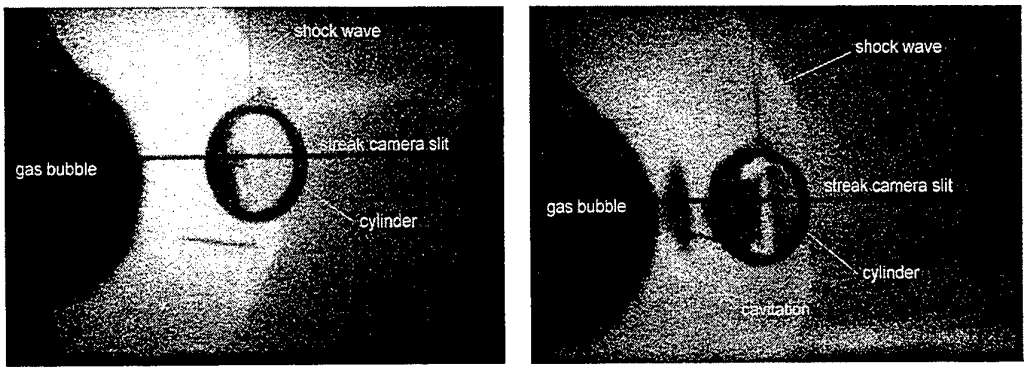

a) b)

Figure 11. Frames showing a shock wave interacting with a cylinder whose longitudinal axis is at 90 deg. to the radial direction of the shock wave (a) 47 and (b) 57 microseconds after detonation of the donor. The mirror period of the Cordin was 467.1 microseconds.

The shock wave interacts with the curved surface of the cylinder and moves around its circumference. A reflected shock wave is formed on contact with the cylinder and is reflected backwards into the bubble of detonation products. There is insufficient detail in the framing records to determine either the formation of Mach stems or associated vortices at the foot of each Mach stem as the shock wave engulfs the cylinder. After the shock wave has passed the cylinder, two distinctive curvatures are seen in the shock wave. The annular silhouette of the cylinder begins to distort, 15 μs after the shock wave interacts with the cylinder. This effect increases during the life time of the experiment until observation through the cylinder becomes totally obscured. No cavitation effects are evident on the surface or in front of the cylinder.

The reflected shock wave interacts with the bubble's surface and cavitation is seen to occur 21 mm from the surface of the bubble and 9.7 microseconds after the shock wave first interacts with the bubble. The formation of cavitation is detailed by the streak record shown in Figure 12. The digitised paths of the shock wave and bubble's surface in the distance-time plane were obtained from the streak record and are shown in Figure 13. Again, the bubble's expansion is retarded by the interaction of the shock wave.

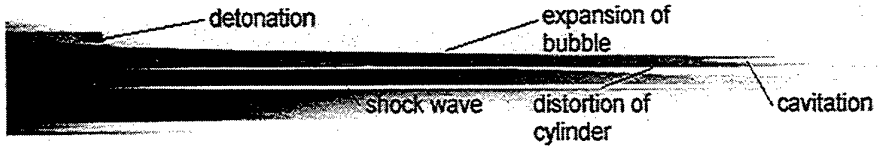

Figure 12. Streak record showing the formation of cavitation, the passage of the shock wave and the motion of the bubble's surface.

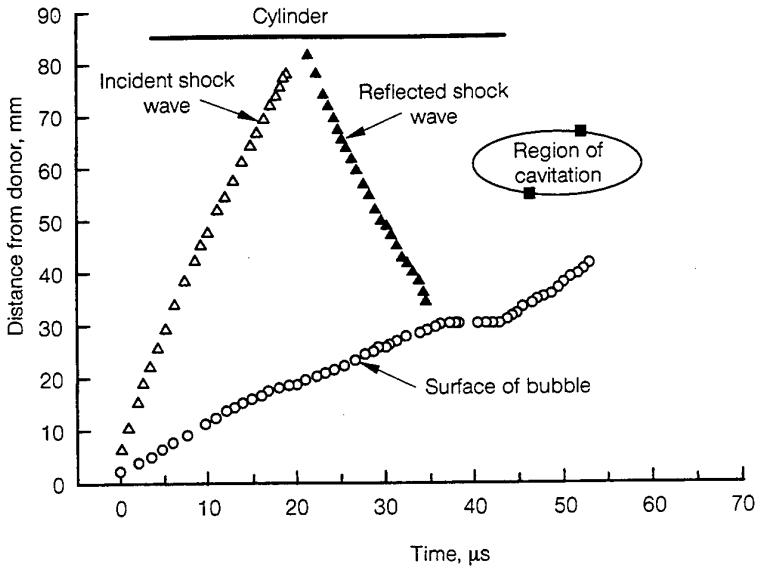

Figure 13. Paths of the shock wave and the surface of the bubble in the s-t plane - Radial interaction.

From Figure 13, the gradient of the distance-time curve indicates that the velocity of the shock wave incident onto the cylinder is 2900 ms^{-1}. Similar calculations to those described above indicate that the pressure and particle velocity in the water in front of the cylinder are 2.1 GPa and 710 ms^{-1} respectively. On impact with the cylinder, the pressure and particle velocity across the boundary are 5.1 GPa and 136 ms^{-1} respectively. Thus, the surface of the cylinder will move backwards with an initial velocity of 136 ms^{-1}. This initial velocity is similar to that for the cylinder described above and one would expect that cavitation would also form on the curved surface of the cylinder. The lack of evidence may be due to the obscuration of cavitation due to the collapse of the cylinder or perhaps cavitation did not occur. As the curved surface of the cylinder would be more rigid than the flat plate at the end of the cylinder, we suspect that the resultant motion of the cylinder was not great enough to reduce the pressure within the water and thus produce cavitation.

Again, the cavitation produced in front of the bubble's surface may be explained in terms of the movement of a free surface and the Hugoniots shown in Figure 3. In this case, the effective loading period of the incident shock wave is 9.7 microseconds.

The complete framing records show the deformation of the cylinder's walls with the passage of the shock wave. The side of the cylinder with which the shock wave first interacts is seen to bulge inwards and the wall opposite, bulges outwards. These effects occur after the passage of the shock wave and are thought to be due to the slow response time of the steel cylinder to events initiated by the shock wave. No evidence is seen of the passage of the shock wave through the air-filled cylinder. The bubble of detonation products reaches the cylinder long after the damage observed to the

cylinder has occurred. The relative position of the cylinder in each frame is constant throughout the period of the experiment.

The deformation of the cylinder and its lack of movement during the passage of the shock wave again indicates that the damage can be associated with the shock wave and not water flow effects. The cylinder was recovered after the experiment and the wall closest to the charge was buckled whilst that furthermost from the charge, ruptured. The cylinder is shown in Figure 14.

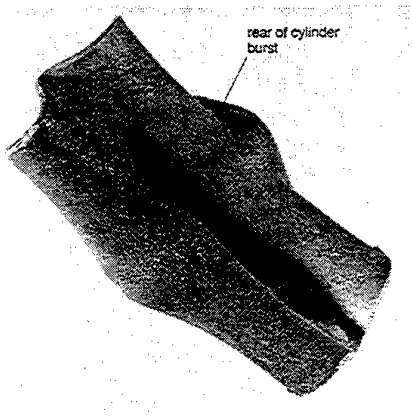

Figure 14. Damage sustained by a cylinder from the passage of a shock wave. Axis of the cylinder is at 90 deg. to the radial direction of the shock wave.

4.2 Detonation of a small cylindrical charge.

The detonation of a small, end initiated cylindrical charge is depicted in Figure 15. The sequence of frames shows that despite the position of the EBW and the shape of the PE4 charge, a few microseconds after detonation the propagating shock wave has developed into a sphere. However, the records show that the bubble of detonation products is affected by the detonator and the bubble does not approach the shape of a spheroid until approximately 100 microseconds after detonation.

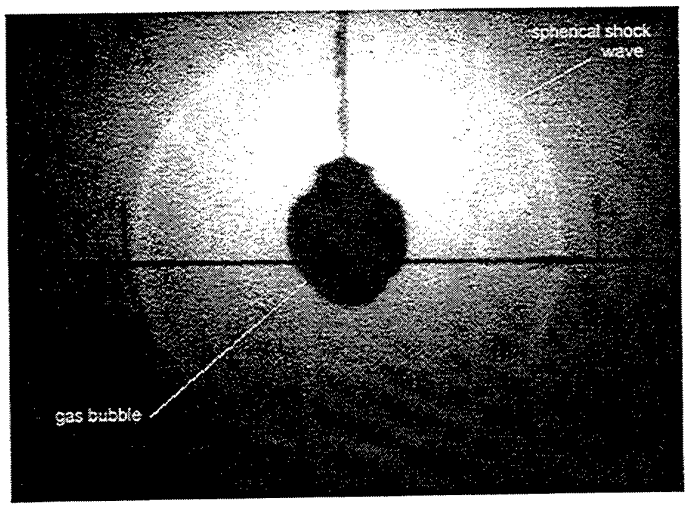

Figure 15. Detonation of an end initiated, right cylinder. The shock wave becomes spherical soon after detonation.

4.3 Cylinders representing sections of a submarine hull.

The interaction of the shock wave produced by the detonation of a small 10 gm charge with a scaled 'submarine cylinder' was imaged with the Cordin camera and selected frames from this record are shown in Figure 16. The low intensity shock wave from the smaller charge makes imaging of the shock wave more difficult. However, as in the previous experiments we see the development of the shock wave, its interaction with and reflection from the target, and the early development of the gas bubble. In addition we observe extensive cavitation at the target surface, much more than was seen in the previous experiments. The shock wave, cavitation, bubble and target response are discussed individually below.

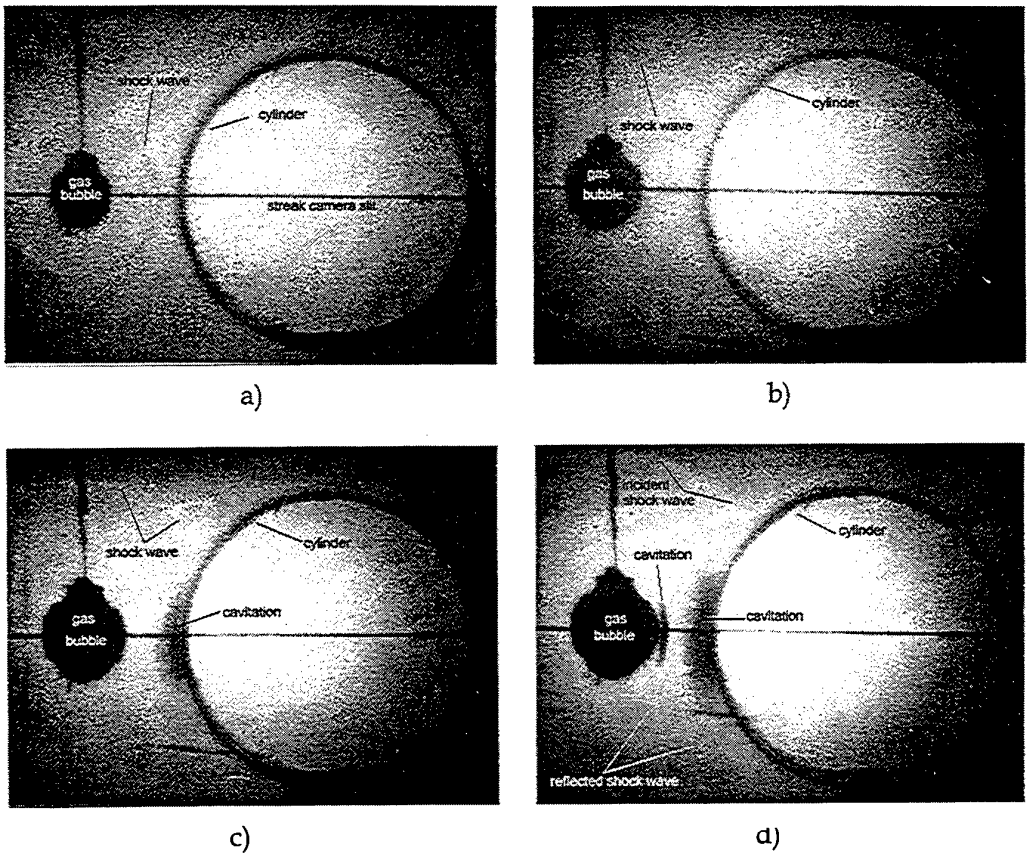

Figure 16. Selected UHS camera frames; a) t = 24 *μs showing shock wave travelling to cylinder, b)* t = 44 *μs, c)* t = 54 *μs showing developing cavitation at cylinder surface, d)* t = 74 *μs showing well developed cavitation off cylinder surface, cavitation off bubble surface and primary and reflected shock waves.*

In the following we analyse our results by comparison to published empirical results for bubble and shock wave parameters. Swisdak [12] presents a convienient compilation of such values for a number of well known explosives. Unfortunately PE4 is not one of these but for our purpose it will suffice to base our analysis on an equivalent mass of TNT which can be derived using the equivalent weight ratios given in Swisdak. We calculate this mass by assuming that PE4 can be characterised as a mixture of 88% RDX and 12% wax. Using this assumption and allowing for the explosive content of the EBW we derive a TNT equivalent mass of 11.5 gms for our PE4 charge.

4.3.1 Shock wave

Examination of Figure 16a to d shows that shortly after detonation the shock wave is clearly visible but at later times its progressive weakening with expansion makes it considerably harder to identify. However, sufficient sections of the expanded initial

shock wave and of the reflected wave can be seen to enable us to trace its subsequent development. For example, close examination of Figure 16d shows the primary shock wave intersecting the cylinder about a quarter of the way around its circumference from the point of first contact. The reflected wave can also be made out, nearly intersecting the centre of the bubble.

Progress of the shock wave can be followed more closely from our streak camera record and the measurements taken from this are shown in Figure 17 for both the shock wave incident on the cylinder and reflected from it. This data has been fitted with 2nd order polynomials, the gradients of which can then be evaluated to give shock wave speeds at any time within the fitted interval. Shortly after detonation (t = 5 μs) the shock wave speed is 3065 ms^{-1} and this gradually decreases to 2452 ms^{-1} at t = 20 μs, with the shock wave reaching the cylinder at t = 26 μs.

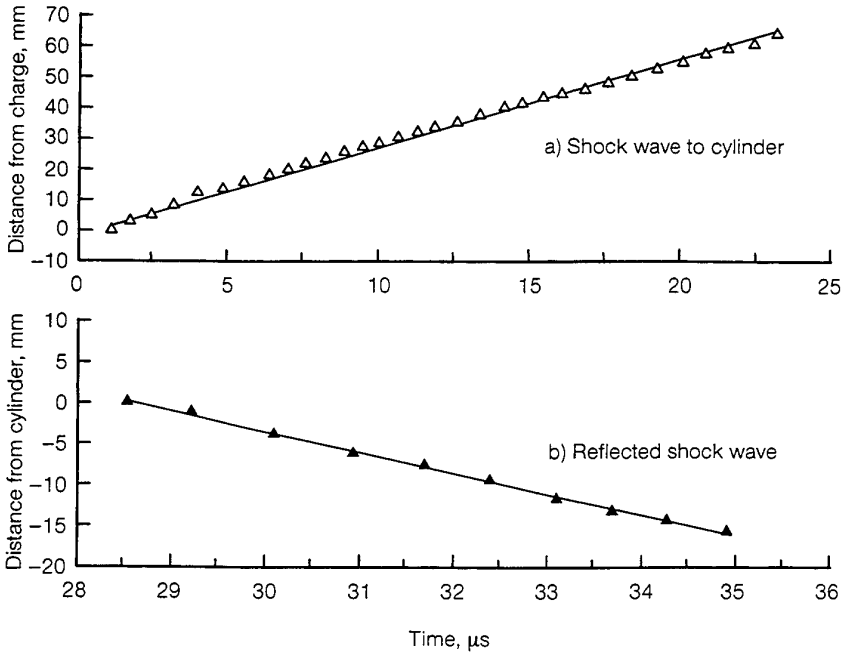

Figure 17. Position of shock waves vs time since detonation. Curves are 2nd order polynomial fits to the data. a) distance from the edge of the charge travelled by initial shock wave, b) distance from the cylinder travelled by reflected shock wave.

For the reflected shock wave we find speed values of 2656 ms^{-1} at t = 30 μs and 2401 ms^{-1} at t = 35 μs. Interestingly the initial speed of the reflected wave is higher than that of the incident wave immediately before it arrives at the cylinder. This can be explained by the dependence of shock wave speed on the density of the transmitting medium. Close to the cylinder the reflected wave is travelling through the denser water still under compression from the tail of the incident wave and consequently its speed can be higher than that of the incident wave travelling through unshocked water.

4.3.2 Cavitation

Clearly visible in Figure 16c is the development of a large region of cavitation off the target surface. This region appears about 16 μs after the shock wave reaches the target and by $t \approx 90$ μs has grown to a maximum size (seen in cross section) which extends about 200 mm perpendicular to the line between the charge and cylinder and about 40 mm between them. Cavitated regions are caused by tension in the water but because the target material is obviously denser than the water we do not expect this cavitation to have been caused by the reflection of a tension wave. Rather we suggest that the tension is set up by the rapid deformation of the cylinder away from the charge and is thus clear evidence that the cylinder is responding to the loading of the incident shock wave.

The occurrence of cavitation modifies the target damage process. Initially it decouples water from the target surface thereby protecting the target from direct loading by the tail of the incident shock wave. The level of shock wave loading protection this supplies can be estimated by comparing the pressure - time curve of the shock wave with the time that cavitation appears. In this experiment we observe the development of cavitation approximately 16 μsecs after arrival of the shock wave at the cylinder surface which corresponds to about 1.2 times the pressure wave time constant (θ) of 13.6 μs calculated from the equations given by Swisdak [12]. The occurrence of pressure cut-off at this time indicates that the cylinder only receives about 60% of the available momentum in the shock wave. Eventually however, we expect the cavitated region to collapse (cavitation closure) and this introduces a second potential damage mechanism associated with the energetic flow of water directed towards the cylinder surface. We see no evidence of this collapse occurring within the short time span imaged by the Cordin camera so we are unable to determine how effective a damage process this will be.

Also clearly seen in Figure 16c is the development of a relatively thin crescent shaped region of cavitation formed off the expanding bubble of detonation products. As was described above the interaction of the reflected compression shock wave from the cylinder with the expanding bubble is expected to give rise to a tension wave reflected off the bubble. Although these waves are too weak to be seen in the photographic record, the shape and timing of formation of this cavitation feature is consistent with it being caused by the passage of such a tension wave.

4.3.3 Bubble

The standard equations for bubble development [12] predict a maximum bubble diameter of 720 mm occurring 68 ms after detonation of a 11.5 gm charge of TNT, so we expect to record only the very early stages of the bubble growth with the Cordin camera. As was mentioned above, to facilitate ease of construction and to ensure detonation, the experimental charge was fashioned as a right cylinder encased in a perspex cover. Consequently, as can be see in Figure 16, the bubble displays some asymmetry in its early stages of growth.

From the streak camera record we have measured the expansion of the bubble surface along the line perpendicular to the cylinder surface and passing through the charge and these measurements are shown in Figure 18.

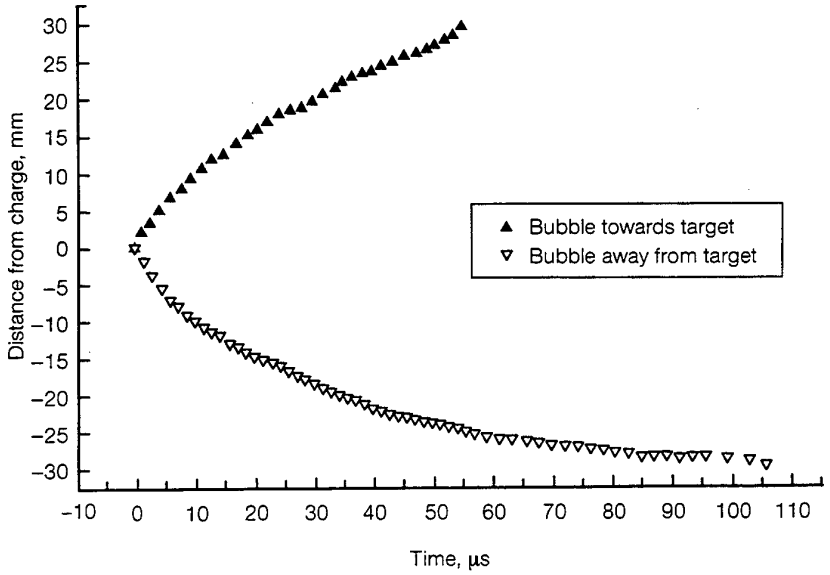

Figure 18. Expansion of the bubble surface (both sides) measured along the line through the charge and perpendicular to the cylinder surface.

During the observed interval the bubble expands to a diameter of about 6 mm which is only a small fraction of the expected maximum diameter but even so the plot of Figure 18 appears to show that the rate of its expansion is already falling off. By the time 50 μs after detonation there is some evidence of a slight asymmetry in the bubble expansion along this axis with the bubble having expanded some 10% further towards the cylinder than away from it. Although this is a small effect it could be a consequence of reduced resistance to water expansion in the direction of the cavitated region formed at the surface of the cylinder.

4.3.4 Target Response

Figure 19 shows the final state of the scaled 'submarine' cylinder. Considerable deformation has occurred - at its maximum value (along the charge - cylinder axis) the cylinder has been reduced to roughly 2/3 of its original diameter. The deformation decreases towards the ends of the cylinder but it is clear that the cylinder is too short to permit us to ignore end effects. Comparison of the cylinders in Figures 16d and 19 shows that very little of the total damage occurs in the first 100 μsecs during the actual shock wave interaction. This result differs to that seen for the 'sea mine' experiments in which considerable damage was seen to occur with the passage of the shock wave.

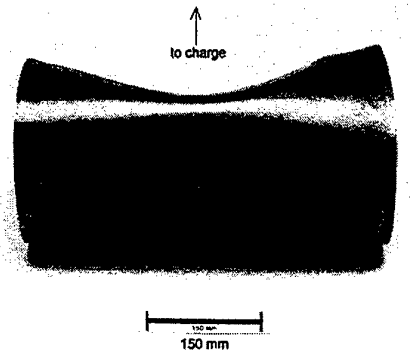

Figure 19. Final state of the scaled 'submarine' cylinder. Axis of the cylinder was perpendicular to the radial direction of the shock wave.

Although this is probably only a consequence of the small charge size coupled with the inertia of the target, it *could* also suggest that the major damage mechanism operating in this low level shock regime is not the direct loading from the shock wave. In a free field environment the process of bubble collapse near or against a target introduces other significant damage mechanisms such as water jet and bubble pulse pressure waves. However, the fragility and dimension of the water tank relative to the maximum bubble diameter are such that these damage mechanisms will have neither time nor water enough to operate. Thus the only other possible causes of the observed damage would be cavitation collapse as discussed above, and the incompressible water flow set up by the passage of the shock wave and the expansion of the bubble. Unfortunately the time span recorded by the Cordin camera is insufficient to observe cavitation collapse or significant expansion of the bubble towards the cylinder, so we cannot determine how important these other possible damage mechanisms were.

If the shock wave is responsible for most of the damage then our results indicate that the cylinder's response to it must occur mostly after our recorded time interval (ie. after 100 μsecs). Some idea of the expected shock wave response can be obtained by applying simple equations for the motion of an infinite free plate (e.g. Cole [2]). Although the geometry of our experiment is obviously not planar we can use these equations to obtain a rough estimate of the expected magnitude of the shock wave response of the cylinder. This estimate will exclude a comparison with possible loading from cavitation collapse but we have seen above that the cavitated region adjacent to the cylinder does not collapse within the recorded interval. For a 11.5 gm charge of TNT detonated 75 mm from a 2.0 mm thick steel plate the predicted maximum velocity is 112 $msec^{-1}$ occurring 12 μsecs after arrival of the shock wave. Treating this as a constant velocity we would expect to see a deformation of only 3.5 mm in the last frame of Figure 8 ($t \approx 74$ μs), which is too small to measure reliably.

We can obtain a much better assessment of the target response by analysis of our streak camera results which record the position of the two narrow sections of cylinder wall crossed by the horizontal axis of the camera. From this we can measure the

displacement of the cylinder wall immediately adjacent to the explosive charge (henceforth referred to as the near side of the cylinder) and of the cylinder wall diametrically opposite this (henceforth referred to as the far side of the cylinder). In Figure 20 we plot the apparent displacement of the inside of these two sections of cylinder wall. The cylinder should be undisturbed until arrival of the shock wave so some idea of the accuracy of these measurements can be obtained from the variation in displacement before $t \approx 26$ μs. Both sections of the wall show a displacement which begins shortly after 40 μs and can be well approximated with straight line fits for $t > 60$ μs giving velocities of 170 ms^{-1} for the far side of the wall and about 270 ms^{-1} for the near side. It should be noticed however that the concurrency of these displacements is inconsistent with the requirement for the shock wave/disturbance to travel the considerable further distance to the far side of the cylinder wall. Because the speed of sound in steel exceeds that in water the quickest possible route for the disturbance to reach the far side of the wall is by travelling through the cylinder wall itself. Assuming the disturbance travels at the speed of sound for steel (≈ 6000 ms^{-1}) we should not expect displacement of the far side to occur until about 70 μs after that of the near side. By this reasoning we are led to the conclusion that the observed displacement of the far side and hence, by implication, at least some of the displacement of the near side is not real and is just an optical effect. We suggest that the most likely explanation for this is that hinging of the cylinder's perspex end caps produces a refraction of the transmitted light from the cylinder walls to the camera thereby producing an apparent and concurrent displacement of both walls of the cylinder. This explanation is supported by the fact that the onset of displacement of the far wall (and the initial displacement of the near wall) is fairly consistent with the expected time of arrival at the perspex end cap of the disturbance which has travelled through the cylinder from the point of shock wave impact at the centre of the cylinder's near side.

Despite this problem we can deduce the real deformation of the cylinder wall by taking the difference between the velocities of the two observed cylinder wall sections. This gives a velocity of deformation for the near side of the cylinder wall of about 90 ms^{-1} which (perhaps suprisingly) is in good agreement with the value predicted by application of the infinite plate theory above. From these results we can say that the deformation of the cylinder within the interval recorded in this experiment is consistent with the expected response to the incident shock wave. This demonstrates that the shock wave interaction is an effective damage mechanism for this target but without knowledge of the target response at later times we cannot be sure that the shock wave alone is capable of inflicting the total damage we see in Figure 19.

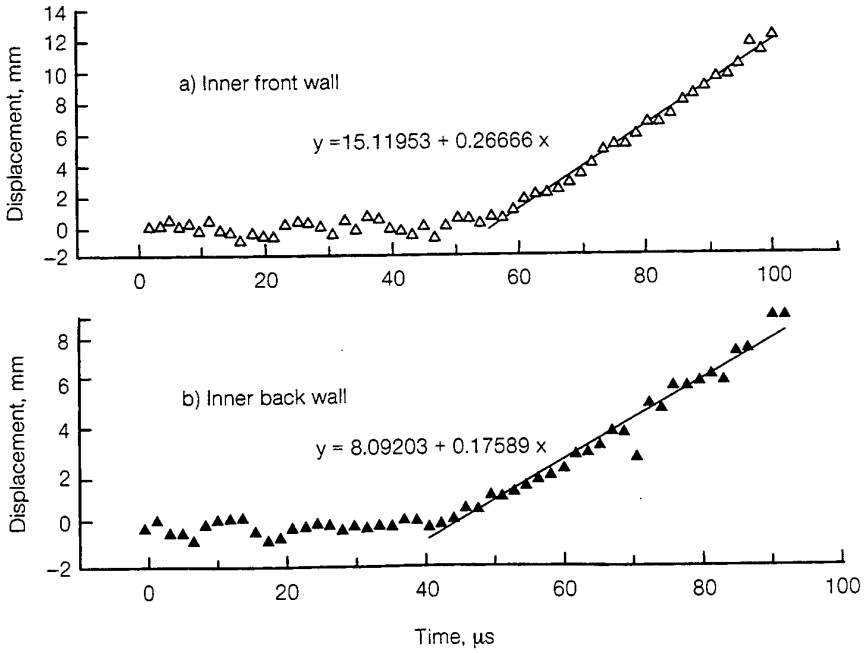

Figure 20. Deflection of the inner wall of the cylinder. a) cylinder wall section immediately adjacent to the explosive charge, b) cylinder wall section diametrically opposite this.

Clearly, filming of the later periods of the interaction would be helpful in investigating the damage process, particularly in regards to cavitation collapse and incompressible water flow. An attempt was made to do this with a slower speed camera but unfortunately this was unsuccessful due to wide spread obscuration of the field of view occurring after a time of 300 μs. This is slightly after the expected time of arrival of the shock wave at the aquarium walls so we believe that the obscuration was caused by cavitation produced by shock wave interaction with the perspex sides of the aquarium test tank. Future experiments will be designed to overcome this limitation.

5. Summary and Conclusions

We have performed experiments utilising ultra high speed photography to study the interaction of shock waves with submerged cylindrical objects. This work was done in support of research tasks on sea mine neutralisation and submarine vulnerability and used appropriately scaled charges and target cylinders.

The first series of experiments focused on sea mine neutralisation and involved relatively large charges and small thick walled cylinders. Our conclusions from this work are:

- Damage to steel cylinders representing sea-mines occurs during the passage of the shock wave, long before the bubble of detonation products expand and contacts the cylinder.
- Because the position of the two cylinders representing sea-mines remain relatively constant through-out the life time of the experiments, the flow effects caused by the passage of the shock wave and expansion of the bubble appear to have little or no effect in the damage process.

The second set of experiments was aimed at investigating the damage *processes* for submarine hulls for which we employed smaller charges and larger thinner walled cylinders. The combination of a smaller charge size and different sized target cylinder to that used for the sea mine study produced a somewhat different response. The results can be summarised as;

- The target cylinder was extensively damaged suffering a reduction in diameter at the centre of about 1/3. Although large this was considerably less severe than that suffered by the equivalent sea mine experiment and occurred less rapidly with the majority of the deformation occurring after passage of the shock wave.

- Although only the beginning of the target deformation was captured by the Cordin camera it was consistent with that expected from shock wave loading so it is clear this is an effective damage mechanism and we suspect that most of the damage can be attributed to it. If so then the slower response to shock loading than seen in the sea mine experiments is just an inertial effect.

- However, extensive cavitation was formed at the cylinder surface. The eventual collapse of such a large region of cavitation can be expected to contribute something to the damage process. Unfortunately the camera record was too short to capture this process so we could not determine how important this contribution was. Further experiments are being conducted to investigate this.

As was discussed in section 3 these results can not be interpreted directly in terms of the response of a real submarine hull. The absence of stiffener rings and the use of mild steel makes the experimental cylinder considerably more responsive than a real submarine hull. The response of more realistic experimental models will be studied in future work but for the moment these current results give some idea of the potential for deformation between the stiffener rings and provide clear experimental results suitable for the development and validation of a computational damage prediction capability.

In a final separate experiment we studied the detonation of a small right cylindrical charge that is commonly used in small scale experiments. We found that the shock wave is spherical. However, in the early stages of its development, the accompanying bubble is not and we conjecture that under greater hydrostatic pressures, the bubble will become spherical as the internal pressures and temperatures within the bubble approach uniform values.

6. References

1. Chung. M.J., McQueen. D., McVay. L., Initiation of Detonation in Composition B by an Underwater Shock Wave, DSTO-TR-0273, Melbourne, Victoria.

2. Cole. R.H., (1948), Underwater Explosions. Princeton University Press, Princeton, New Jersey.

3. HULVUL Trial, Private communication with N. Burman

4. USS Roberts, Private communication with N Burman

5. R14 Special, Private communication from Kavetsky, R, NSWC White Oak.

6. Best. J. P., (1993). The Formation of Toroidal Bubbles upon the Collapse of Transient Cavities. J. Fluid Mech. vol. 251, pp 79-107.

7. Duvall, G. F., Fowles, R. (1963). Chapter 9, Shock Waves, ed. R. S. Bradley, Academic Press, London.

8. Liddiard, T. P., Forbes, J. W. (1987). A Summary Report of the Modified Gap Test and the Underwater Sensitivity Test, NSWC TR 86-350, Naval Surface Warfare Center, Dahlgren, Virginia.

9. Marsh, S. P. (ed.) (1980). LASL Shock Hugoniot Data, University of California Press, Berkeley.

10. Rice, M.H., Walsh, J. M. (1957). Equation of State of Water to 250 Kilobars, The Journal of Chemical Physics, Vol. 26, No. 4.

11. Chung, M.J., Kinsey. T. A Study of Underwater Blast Effects on Simple Structures, Shielded and Bare Explosive Materials. Paper submitted to the Fourth International Symposium on Behaviour of Dense Media under High Dynamis Pressures, Tours, France.

12. Swisdak, M. (1978). Explosive Effects and Properties II. Explosive Effects in Water. NSWC/WOL/TR 76 116.

DISTRIBUTION LIST

Assessment of Underwater Blast Effects on Scaled, Submerged Cylindrical Objects

Michael Chung and John Brett

AUSTRALIA

DEFENCE ORGANISATION

Task Sponsor Submarine Project Directorate (Att. Mr P. Hugonnet)
APW 1-5-29

S&T Program

Chief Defence Scientist
FAS Science Policy
AS Science Corporate Management
} shared copy

Director General Science Policy Development
Counsellor Defence Science, London (Doc Data Sheet)
Counsellor Defence Science, Washington (Doc Data Sheet)
Scientific Adviser to MRDC Thailand (Doc Data Sheet)
Director General Scientific Advisers and Trials/Scientific Adviser Policy and Command
(shared copy)
Navy Scientific Adviser (Doc Data Sheet and distribution list only)
Scientific Adviser - Army (Doc Data Sheet and distribution list only)
Air Force Scientific Adviser
Director Trials

Aeronautical and Maritime Research Laboratory
Director

Chief of Maritime Platforms Division
Lincoln Wood RLMSS (MPD)
David Thompson RLMWS (WSD)
Norbert Burman (MPD)
Michael Chung
John Brett
David Ritzel
David Jones

DSTO Library
Library Fishermens Bend
Library Maribyrnong
Library Salisbury (2 copies)
Australian Archives
Library, MOD, Pyrmont (Doc Data sheet only)

Capability Development Division
Director General Maritime Development
Director General Land Development (Doc Data Sheet only)
Director General C3I Development (Doc Data Sheet only)

Navy
SO (Science), Director of Naval Warfare, Maritime Headquarters Annex,
Garden Island, NSW 2000 (Doc Data Sheet only)

Operations Requirements Manager, MHCP, CP2-3-14

Army

ABCA Office, G-1-34, Russell Offices, Canberra (4 copies)
SO (Science), DJFHQ(L), MILPO Enoggera, Queensland 4051 (Doc Data Sheet only)
NAPOC QWG Engineer NBCD c/- DENGRS-A, HQ Engineer Centre Liverpool Military Area, NSW 2174 (Doc Data Sheet only)

Intelligence Program

DGSTA Defence Intelligence Organisation

Corporate Support Program (libraries)

OIC TRS, Defence Regional Library, Canberra
Officer in Charge, Document Exchange Centre (DEC), 1 copy
*US Defence Technical Information Center, 2 copies
*UK Defence Research Information Centre, 2 copies
*Canada Defence Scientific Information Service, 1 copy
*NZ Defence Information Centre, 1 copy
National Library of Australia, 1 copy

UNIVERSITIES AND COLLEGES

Australian Defence Force Academy
Library
Head of Aerospace and Mechanical Engineering
Deakin University, Serials Section (M list), Deakin University Library, Geelong, 3217 Senior Librarian, Hargrave Library, Monash University
Librarian, Flinders University

OTHER ORGANISATIONS

NASA (Canberra)
AGPS

OUTSIDE AUSTRALIA

ABSTRACTING AND INFORMATION ORGANISATIONS

INSPEC: Acquisitions Section Institution of Electrical Engineers
Library, Chemical Abstracts Reference Service
Engineering Societies Library, US
Materials Information, Cambridge Scientific Abstracts, US
Documents Librarian, The Center for Research Libraries, US

INFORMATION EXCHANGE AGREEMENT PARTNERS

Acquisitions Unit, Science Reference and Information Service, UK
Library - Exchange Desk, National Institute of Standards and Technology, US

SPARES (10 copies)

Total number of copies: 59

DEFENCE SCIENCE AND TECHNOLOGY ORGANISATION
DOCUMENT CONTROL DATA

1. PRIVACY MARKING/CAVEAT (OF DOCUMENT)

2. TITLE

Assessment of Underwater Blast Effects on Scaled, Submerged Cylindrical Objects

3. SECURITY CLASSIFICATION (FOR UNCLASSIFIED REPORTS THAT ARE LIMITED RELEASE USE (L) NEXT TO DOCUMENT CLASSIFICATION)

Document	(U)
Title	(U)
Abstract	(U)

4. AUTHOR(S)

Michael Chung and John Brett

5. CORPORATE AUTHOR

Aeronautical and Maritime Research Laboratory
PO Box 4331
Melbourne Vic 3001 Australia

6a. DSTO NUMBER	6b. AR NUMBER	6c. TYPE OF REPORT	7. DOCUMENT DATE
DSTO-TR-0575	AR-010-327	Technical Report	September 1997

8. FILE NUMBER	9. TASK NUMBER	10. TASK SPONSOR	11. NO. OF PAGES	12. NO. OF REFERENCES
510/207/0315	94/135	NAV-SPO	24	12

13. DOWNGRADING/DELIMITING INSTRUCTIONS

None

14. RELEASE AUTHORITY

Chief, Maritime Platforms Division

15. SECONDARY RELEASE STATEMENT OF THIS DOCUMENT

Approved for public release

OVERSEAS ENQUIRIES OUTSIDE STATED LIMITATIONS SHOULD BE REFERRED THROUGH DOCUMENT EXCHANGE CENTRE, DIS NETWORK OFFICE, DEPT OF DEFENCE, CAMPBELL PARK OFFICES, CANBERRA ACT 2600

16. DELIBERATE ANNOUNCEMENT

No Limitations

17. CASUAL ANNOUNCEMENT Yes

18. DEFTEST DESCRIPTORS

Underwater explosions: Blast Effects: Shockwaves: Explosive charges: Water flow.

19. ABSTRACT

The underwater detonation of large explosive charges close by a target, produce effects that are devastating to vessels such as ships and submarines and in addition, provide a means to neutralise threat sea-mines. The roles of the underwater shock wave, flow and bubble in the damage process are not as yet, clear. We present results of an experimental study visualising the effects of underwater explosions on scaled, submerged cylindrical objects that represent submarines and sea-mines. Significant structural damage to the cylinder occurred with the passage of the shock wave. During this period, the bubble of detonation products failed to expand sufficiently to contact the cylinder. Some evidence is available to suggest that the principal damage mechanism can be attributed to shock wave interaction and not water flow effects. Cavitation was created by the response of the cylinder to the shock wave and by the reflection of the shock wave from the bubble. Estimation of the effective loading period of the shock wave was made from these effects.